

Fast Coherent Point Drift

Xiang-Wei Feng^{1,*}, Da-Zheng Feng¹, Yun Zhu²

1, National Laboratory of Radar Signal Processing, Xidian University, Xi'an, China

2 School of Computer Science, Shaanxi Normal University, Xi'an, China

Corresponding author: Xiang-Wei Feng (e-mail: fengxiangwei@stu.xidian.edu.cn).

Abstract: Nonrigid point set registration is widely applied in the tasks of computer vision and pattern recognition. Coherent point drift (CPD) is a classical method for nonrigid point set registration. However, to solve spatial transformation functions, CPD has to compute inversion of a $M \times M$ matrix per iteration with time complexity $O(M^3)$. By introducing a simple corresponding constraint, we develop a fast implementation of CPD. The most advantage of our method is to avoid matrix-inverse operation. Before the iteration begins, our method requires to take eigenvalue decomposition of a $M \times M$ matrix once. After iteration begins, our method only needs to update a diagonal matrix with linear computational complexity, and perform matrix multiplication operation with time complexity approximately $O(M^2)$ in each iteration. Besides, our method can be further accelerated by the low-rank matrix approximation. Experimental results in 3D point cloud data show that our method can significantly reduce computation burden of the registration process, and keep comparable performance with CPD on accuracy.

Keywords: Point set registration, nonrigid, coherent point drift, matrix inversion, fast algorithm

I. Introduction

The nonrigid point registration is an important technique in the fields of computer vision and pattern recognition. It has been broadly applied in image retrieval, medical image processing, 3D reconstruction, face alignment, and so on. Suppose that there are two point sets that are denoted as the model point set $\mathbf{X} = (\mathbf{x}_1^T, \mathbf{x}_2^T, \dots, \mathbf{x}_M^T)^T \in \mathbb{R}^{M \times D}$, and the scene point set $\mathbf{Y} = (\mathbf{y}_1^T, \mathbf{y}_2^T, \dots, \mathbf{y}_N^T)^T \in \mathbb{R}^{N \times D}$, respectively. The aim of nonrigid point registration method is to recover the spatial transformation between the two point sets. Many methods were developed under the iterative scheme that contains two closely coupled substeps: establish the correspondences, and recover the spatial transformation.

The iterative closest point (ICP) algorithm [1-2] is the most popular method for point set registration. It is simple, general and efficient. Based on nearest neighbor strategy, ICP establishes a binary matrix to represent the corresponding relationship between point sets. However, ICP requires that the initial positions of the point sets are close enough. Otherwise, it easily gets stuck into a poor local minimum.

By replacing the nearest neighbor strategy into softassign, TPS-RPM (Thin plate spline - Robust point matching) was developed in [3-4]. Softassign relaxes the binary constraint of ICP, and uses continuous values to represent point-to-point corresponding relationship. This can improve the robustness of the registration methods by making optimization process be continuous, rather than jumping in binary variables with great arbitrariness. Another impressive work is coherent point drift (CPD) [5], and an improved version in [6]. Based on motion coherence theory (MCT) and Gaussian Mixture Models (GMM), CPD used maximum likelihood estimation (MLE) to model the alignment of two point sets, and employed an Expectation-Maximization (EM) scheme to solve the problem. Both TPS-RPM and CPD adopt the same cost function and a similar alternating update strategy [7]. The main difference between them is that TPS-RPM uses TPS as the transformation function, and CPD uses Gaussian radial basis functions (GRBF). The parameters of TPS can be explicitly decomposed into rigid and nonrigid parts. But TPS does not exist in 4D and higher dimensions, while GRBF can be easily extended into any dimension. By refining the point distribution models, non-uniform Gaussian mixture models [8], asymmetric Gaussian mixture models [9], and Student's-t mixture models [10], are introduced to substitute GMMs to achieve the point set registration.

Recently, many works were developed on the basis of TPS-RPM and CPD. The first strategy is to estimate the correspondences by fusing various structural features, and the second is to introduce spatially constraints to preserve local structural topology (LSD). The above two strategies can be utilized together. In [11]-[16], the local structural descriptors, such as shape context (SC) [17], the inner distance based context descriptor (IDSC) [18], Fast Point Feature Histograms (FPFH) [19], and the three-dimensional context descriptor (3DSC) [20], or self-designed shape descriptors are exploited as an auxiliary to search the corresponding relationship. The motivation of the second strategy is that the neighborhood structure of a point is generally well preserved because of physical constraints [11]. In [11], the authors interpreted the neighboring points as a simple graph, and preserved local structures by maximizing the number of matched edges. In [21], the authors used a

weighted least square error item to represent the connections of k-connected neighboring points. In [22]-[25] and [14], the classical manifold regularization techniques, such locally linear embedding (LLE), local preserving projections (LPP), Laplacian eigenmaps (LE), were employed to maintain stability of local structures in registration process. Although these methods can utilize local structural features more efficiently, there are two problems: first, the computational complexity would increase; second, they are sensitive to outliers because outliers would seriously affect the descriptions of local structures. Besides, by recasting the two point sets as two continuous densities using GMM, [7] and [26]-[29] reported a kind of novel methods that accomplished the nonrigid registration by minimizing the discrepancy between them. Limited by the length of the article, many excellent works are not introduced in our paper. More other works can refer to the good reviews [30]-[31].

The previous works are constructive and notable. However, the computational burden of the nonrigid point registration is still too heavy in large-scale problems. Roughly, there are two kinds of spatial transformation, which are the rigid and nonrigid. The rigid transformation contains translation, rotation and scaling. It can be modeled with few parameters. Correspondingly, a small number of correspondences can well recover the rigid transformation. Compared with rigid transformation, nonrigid transformation has two properties: First, the nonrigid transformation is nonlinear and arbitrary. In order to well fit the complex nonrigid transformation, we have to adopt complicated interpolation functions. These functions usually possess a number of free parameters to be solved. Second, in different local regions, the nonrigid transformation is likely to vary dramatically. Thus, in order to well represent the subtle changes, a number of controlling points have to be extracted from the naive images. These two properties would increase the computational burden.

To address this issue, we develop a fast method to significantly improve the computational efficiency of CPD, which is named fast-CPD. The computational bottleneck for CPD is in solving the transformation function. It has to calculate the inversion of a $M \times M$ matrix with time complexity $O(M^3)$ per iteration. The computational burden is too heavy if there are a large number of feature points to be matched. Compared with CPD, we introduce a corresponding constraint to force each model point to search its corresponding point in the scene point set. Based

on this constraint, we can obtain the solutions of transformation function by updating a diagonal matrix with linear computational complexity, and taking matrix multiplication operation with approximately $O(M^2)$. Although we need to take eigenvalue decomposition of a $M \times M$ matrix once before the iteration begins, the computational cost can be significantly saved because matrix-inverse operation can be avoided in each iteration. Besides, like CPD, the computational cost of our method can be further reduced by using low-rank matrix approximation.

The rest of the paper is organized as follows: In Section II, we introduce the models for nonrigid point set registration. Section III details the fast implementations, low-rank approximation, and the relations between CPD and our method. In Section IV, we present the experimental results. Section V concludes this paper.

II. Models

The point features, including edges [32], corners [33], SIFT [34], ORB [35] and so on, are extracted from the corresponding images. The point sets can be regarded as the simplified representations of the images because abundant structural information and geometric characteristics are preserved. In practice, the point sets can be utilized to recover the spatial transformation between two images, which can significantly save the computational cost, and avoid the effects of pixel intensity changes, such as the illumination changes. However, because of scene variations, pollutions of the naive images, and limitations of point feature extractors, the degradations, such as noise, outlier, and occlusion, inevitably exist in the point sets. They can seriously break the structures in some local areas, which would make it be difficult to obtain adequate reliable one-to-one correspondences. To address this issue, the probability-based methods are developed, and have achieved good performance in accuracy. CPD is one of the representative probability-based works. Here, we briefly introduce the theory and the optimization scheme of CPD.

Given two point sets (the model point set $\mathbf{X} \in \mathbb{R}^{M \times D}$, and the scene point set $\mathbf{Y} \in \mathbb{R}^{N \times D}$), the ultimate goal is to search the interpolation functions $f(\mathbf{X}; \boldsymbol{\theta})$ to recover the spatial transformation from \mathbf{X} to \mathbf{Y} , where $\boldsymbol{\theta}$ denotes the parameters of the interpolation functions. For convenience, we use $\tilde{\mathbf{x}}_m = f(\mathbf{x}_m; \boldsymbol{\theta})$ to denote the new position of \mathbf{x}_m after transformation. In the probability-based methods, the point set registration problems are recast to a probability density estimation

problem based on Gaussian mixture models (GMM). The model points are served as the centroids of GMMs. The probability distribution of the scene points can be represented as a linear combination of GMMs [36], which is denoted as

$$p(\mathbf{y}_n) = \sum_{m=1}^M \pi_m g(\mathbf{y}_n; \tilde{\mathbf{x}}_m, \sigma^2 \mathbf{I}) + \pi_{M+1}, \quad (1)$$

where $g(\mathbf{y}_n; \tilde{\mathbf{x}}_m, \sigma^2 \mathbf{I}) = \frac{1}{(2\pi\sigma^2)^{D/2}} \exp\left(-\frac{\|\mathbf{y}_n - \tilde{\mathbf{x}}_m\|^2}{2\sigma^2}\right)$, and π_m is the probability that \mathbf{y}_n is

assigned to the m -th distribution. In CPD, equal probabilities are assigned between \mathbf{y}_n and the GMM components, which is denoted as $\pi_m = 1/M$, where $m = 1, \dots, M$. In order to deal with noise and outliers, an extra term is added, which is denoted as $\pi_{M+1} = 1/N$. An empirical parameter ω ($0 \leq \omega \leq 1$) is used to represent the relation between \mathbf{y}_n and the extra uniform distribution.

Therefore, equation (1) can be rewritten as

$$p(\mathbf{y}_n) = \frac{\omega}{N} + \frac{(1-\omega)}{M} \sum_{m=1}^M g(\mathbf{y}_n; \tilde{\mathbf{x}}_m, \sigma^2 \mathbf{I}). \quad (2)$$

Based on the *i.i.d.* data assumption, the log-likelihood function can be denoted as

$$\ln p(\mathbf{Y}) = \sum_{n=1}^N \ln \left[\frac{\omega}{N} + \frac{(1-\omega)}{M} \sum_{m=1}^M g(\mathbf{y}_n; \tilde{\mathbf{x}}_m, \sigma^2 \mathbf{I}) \right]. \quad (3)$$

The nonrigid point set registration can be accomplished by maximizing equation (3) using the famous EM (Expectation-Maximum) algorithm, which can be briefly written as follows,

E-step: Compute the correspondence matrix $\mathbf{P} = \{p_{mn}\}_{M \times N}$, which can be denoted as

$$p_{mn} = \exp\left(-\frac{\|\mathbf{y}_n - \tilde{\mathbf{x}}_m\|^2}{2\sigma^2}\right) / \left[\sum_{k=1}^M \exp\left(-\frac{\|\mathbf{y}_n - \tilde{\mathbf{x}}_k\|^2}{2\sigma^2}\right) + c \right], \quad (4)$$

where $c = (2\pi\sigma^2)^{D/2} \frac{\omega}{1-\omega} \frac{M}{N}$. Notably, in our paper, we introduce a corresponding constraint,

which is expressed as

$$\sum_{n=1}^N p_{mn} = 1. \quad (5)$$

Equation (5) means that each model point has to search its corresponding point in the scene point set.

M-step: Calculate the spatial transformation by minimizing the following energy function, which can be represented by

$$Q(\boldsymbol{\theta}, \sigma^2) = \frac{1}{2\sigma^2} \sum_{n=1}^N \sum_{m=1}^M p_{mn} \| \mathbf{y}_n - f(\mathbf{x}_m, \boldsymbol{\theta}) \|^2 + \frac{MD}{2} \ln \sigma^2. \quad (6)$$

In order to smooth the interpolation function to avoid over-arbitrary spatial transformation, a regularization term can be introduced in equation (6) according to the Tikhonov regularization theory [37], which is defined as

$$Q(\boldsymbol{\theta}, \sigma^2) = \frac{1}{2\sigma^2} \sum_{n=1}^N \sum_{m=1}^M p_{mn} \| \mathbf{y}_n - f(\mathbf{x}_m, \boldsymbol{\theta}) \|^2 + \frac{MD}{2} \ln \sigma^2 + \frac{\lambda}{2} \varphi(f) \quad (7)$$

Through iteratively running E-step and M-step, equation (3) can be gradually maximized. The final results can be employed to recover the spatial transformation.

III. Fast Optimization of M-step

Usually, it needs $O(MN)$ operations to calculate the correspondences in E-step, and fast Gaussian transform (FGT) can further reduce the computational complexity to $O(M + N)$. The computational cost for correspondence is acceptable in practice. Besides, it can be further accelerated by parallel computation on GPU devices. Therefore, we focus on how to reduce the computational burden on calculating the spatial transformation in M-step. Herein, by preserving the terms that are only related to the transformation function f , we rewrite equation (7) as

$$Q_f(\boldsymbol{\theta}) = \frac{1}{2\sigma^2} \sum_{n=1}^N \sum_{m=1}^M p_{mn} \| \mathbf{y}_n - f(\mathbf{x}_m, \boldsymbol{\theta}) \|^2 + \frac{\lambda}{2} \varphi(f). \quad (8)$$

The new location is defined as the sum between the initial location and a displacement function v based on Motion Coherent Theory (MCT) [38] [39], which is denoted as

$$f(\mathbf{X}) = \mathbf{X} + v(\mathbf{X}). \quad (9)$$

The regularization of the displacement function can be modeled in the Reproducing Kernel Hilbert Space (RKHS). By using calculus of variation, the optimal displacement function with respect to equation (8) can be defined as the linear combinations of Gaussian kernel functions, which is denoted as

$$v(\mathbf{x}) = \sum_{m=1}^M \mathbf{w}_m \phi(\mathbf{x}, \mathbf{x}_m), \quad (10)$$

where $\phi(\mathbf{x}, \mathbf{x}_m) = \exp(-\|\mathbf{x} - \mathbf{x}_m\|^2 / 2\beta^2) \mathbf{I}_{D \times D}$, and $\mathbf{I}_{D \times D}$ is an $D \times D$ identity matrix. Equation (8) can be rewritten as follows

$$Q_f(\mathbf{W}) = \frac{1}{2\sigma^2} \sum_{n=1}^N \sum_{m=1}^M p_{mn} \| \mathbf{y}_n - (\mathbf{x}_m + \boldsymbol{\Phi}_m \mathbf{W}) \|^2 + \frac{\lambda}{2} \text{tr}(\mathbf{W}^T \boldsymbol{\Phi} \mathbf{W}), \quad (11)$$

where $\Phi = \left(\exp\left(-\|\mathbf{x}_i - \mathbf{x}_j\|^2 / 2\beta^2\right) \right) \in \mathbb{R}^{M \times M}$ is a symmetric Gram matrix, and $\phi_m \in \mathbb{R}^{1 \times M}$ is the m -th row of Φ . Letting $\frac{\partial Q_f(\mathbf{W})}{\partial \mathbf{W}^T} = 0$ yield

$$-\frac{1}{\sigma^2} \sum_{m=1}^M \phi_m^T \sum_{n=1}^N p_{mn} \mathbf{y}_n + \frac{1}{\sigma^2} \sum_{m=1}^M \phi_m^T \mathbf{x}_m \sum_{n=1}^N p_{mn} + \frac{1}{\sigma^2} \sum_{m=1}^M \phi_m^T \phi_m \mathbf{W} \sum_{n=1}^N p_{mn} + \lambda \Phi \mathbf{W} = \mathbf{0}. \quad (12)$$

According to the corresponding constraint $\sum_{n=1}^N p_{mn} = 1$, it can deduce

$$-\sum_{m=1}^M \phi_m^T \tilde{\mathbf{y}}_m + \sum_{m=1}^M \phi_m^T \mathbf{x}_m + \sum_{m=1}^M \phi_m^T \phi_m \mathbf{W} + \lambda \sigma^2 \Phi \mathbf{W} = \mathbf{0}, \quad (13)$$

where $\tilde{\mathbf{y}}_m = \sum_{n=1}^N p_{mn} \mathbf{y}_n$ can be seen as the newly estimated position that is corresponding to \mathbf{x}_m using scene point sets. The compact form of equation (13) can be denoted as

$$\Phi^T \Phi \mathbf{W} + \lambda \sigma^2 \Phi \mathbf{W} = \Phi^T \tilde{\mathbf{Y}} - \Phi^T \mathbf{X}, \quad (14)$$

where $\tilde{\mathbf{Y}}$ is the data matrix that are formed by $\{\tilde{\mathbf{y}}_n\}$. Because Φ is symmetric, we have $\Phi^T = \Phi$.

Therefore, the equation (14) can be simplified as

$$\left(\Phi + \lambda \sigma^2 \mathbf{I}_{M \times M} \right) \mathbf{W} = \tilde{\mathbf{Y}} - \mathbf{X}, \quad (15)$$

where $\mathbf{I}_{M \times M}$ is an $M \times M$ identity matrix. By taking eigenvalue decomposition of $\Phi = \mathbf{U} \mathbf{\Lambda} \mathbf{U}^T$, it can be obtained

$$\mathbf{U} \left(\mathbf{\Lambda} + \lambda \sigma^2 \mathbf{I}_{M \times M} \right) \mathbf{U}^T \mathbf{W} = \tilde{\mathbf{Y}} - \mathbf{X}. \quad (16)$$

Because $\mathbf{U}^T = \mathbf{U}^{-1}$, the solution of \mathbf{W} can be denoted as

$$\mathbf{W} = \mathbf{U} \left(\mathbf{\Lambda} + \lambda \sigma^2 \mathbf{I}_{M \times M} \right)^{-1} \mathbf{U}^T \left(\tilde{\mathbf{Y}} - \mathbf{X} \right). \quad (17)$$

Notably, using equation (17) to calculate \mathbf{W} , we only need to update a diagonal matrix

$\left(\mathbf{\Lambda} + \lambda \sigma^2 \mathbf{I}_{M \times M} \right)^{-1}$ with linear computational complexity, and to take matrix multiplication operations.

It totally needs $O(2DM^2 + DM + M)$ operations. Because $D \ll M$, our method can significantly improve the computational efficiency of nonrigid point registration. Besides, the σ^2 can be calculated as

$$\sigma^2 = \frac{1}{DM} \sum_{n=1}^N \sum_{m=1}^M \|\mathbf{y}_n - f(\mathbf{x}_m, \mathbf{W})\|^2 = \frac{1}{DM} \left(\text{tr}(\mathbf{Y}^T \mathbf{d}(\mathbf{P}^T \mathbf{1}) \mathbf{Y}) - 2\text{tr}(\tilde{\mathbf{Y}}^T \tilde{\mathbf{X}}) + \text{tr}(\tilde{\mathbf{X}}^T \tilde{\mathbf{X}}) \right), \quad (18)$$

where $\tilde{\mathbf{X}} = f(\mathbf{X}, \mathbf{W})$ is the transformed model point set and $\mathbf{d}^{-1}(\cdot)$ denotes the inverse diagonal matrix.

Low-rank approximation: Equation (17) can be further accelerated by low-rank approximation. By preserving the principal components of matrix Φ , the approximation reconstruction of Φ can be denoted as

$$\tilde{\Phi} = \tilde{\mathbf{U}}\tilde{\Lambda}\tilde{\mathbf{U}}^T, \quad (19)$$

$\tilde{\Lambda} \in \mathbb{R}^{K \times K}$ is composed by the K largest eigenvalues of the matrix Φ , and $\tilde{\mathbf{U}} \in \mathbb{R}^{M \times K}$ is formed by corresponding eigenvectors. Therefore, the approximation solution $\tilde{\mathbf{W}}$ can be denoted as

$$\tilde{\mathbf{W}} = \tilde{\mathbf{U}}(\tilde{\Lambda} + \lambda\sigma^2\mathbf{I}_{K \times K})^{-1}\tilde{\mathbf{U}}^T(\tilde{\mathbf{Y}} - \mathbf{X}). \quad (20)$$

The computational complexity of equation (20) is $O(2DKM + DK + K)$ operations. If there are an amount of feature points and the shape of the point cloud is well persevered, we can choose $K \ll M$, which can further reduce the computational burden to be approximately linear.

Relationship with CPD: Our method can be simply seen as a fast implementation of CPD so that we have to claim that our method is very likely to CPD, including the theory, cost function and optimization scheme. The main difference is on calculating the spatial transformation. In CPD, the spatial transformation is calculated by

$$\mathbf{W}_{cpd} = (\Phi + \lambda\sigma^2\mathbf{d}(\mathbf{P}\mathbf{1})^{-1})^{-1}(\mathbf{d}(\mathbf{P}\mathbf{1})^{-1}\mathbf{P}\mathbf{Y} - \mathbf{X}). \quad (21)$$

As shown in equation (21), CPD has to calculate the inversion of a $M \times M$ matrix with time complexity $O(M^3)$. Through introducing the corresponding constraint, our method can get the solutions by updating a diagonal matrix with linear computational complexity, and taking matrix multiplication operation. The matrix-inverse operation is avoided so that the computational burden can be significantly reduced.

IV. Experiments

Our method is implemented in MATLAB, and the experimental environment is an Intel Core i7-8750H CPU and 32GB RAM. Our method can be simply treated as a fast implementation of CPD. Besides, the CPD-based methods can be easily accelerated by our method with minor modification. Therefore, the experiments focus on comparing the time cost and the accuracy between CPD and ours. Besides, we also test another recently CPD-based point set registration algorithm that has publicly

available codes that are provided by the authors, which is GLTP [Song, 2019]. On the scheme of CPD, GLTP employs the LLE technique to preserve local structures.

Evaluation Criterion: We use two experiments to verify the performance of the algorithms. In the first experiment, we adopt the wolf dataset to compare the abilities of the algorithms when confronted with various data degradations, including nonrigid deformation, noise, occlusion and outliers. Besides, we also compare the runtime of the methods. The second experiment focus on comparing the computational efficiency between CPD, CPD(low-rank), fast-CPD and fast-CPD(low-rank) using the bunny dataset. For convenience, we denote CPD(low-rank) and fast-CPD(low-rank) as CPD-L and fast-CPD-L, respectively.

1) Accuracy: The root-mean-square error (RMSE) is used as the registration error, which is denoted as follows,

$$RMSE = \sqrt{\frac{1}{M} \sum_{m=1}^M \|f(\mathbf{x}_m) - \hat{\mathbf{y}}_m\|^2}, \quad (22)$$

where $\hat{\mathbf{y}}_m$ is the ground truth corresponding point of \mathbf{x}_m .

2) Runtime: The total runtime t_{total} of the methods can be roughly divided into three parts: the time t_c to calculate the correspondences, the time t_f to compute the spatial transformation, and the time t_o for other operations in the programs, and $t_{total} = t_c + t_f + t_o$. For fast-CPD, CPD-L, and fast-CPD-L, t_f is composed by the time t_{eig} to take eigenvalue decomposition of the $\Phi \in \mathbb{R}^{M \times M}$ before the iteration begins, and the time t_{iter} to compute the spatial transformation in the iterations, and $t_f = t_{eig} + t_{iter}$. Specially, for CPD and GLTP, there are $t_{eig} = 0$, and $t_f = t_{iter}$.

Note: Compared with naive CPD, fast-CPD only additionally performs a normalization operation as equation (5) with linear computational complexity for computing the correspondences. Besides, the cost time for correspondence determination can be significantly reduced by FGT (Fast Gaussian Transform) and parallel computing on GPU devices. Because it does not belong to the research scope of this paper, we do not specially accelerate the step of correspondence determination. The main difference between fast-CPD and CPD is how to compute the spatial transformation. Therefore, we take t_f as the key metric to evaluate the computational efficiency of various registration methods.

Parameter settings: The free parameters of CPD and fast-CPD are same, including the noise and outlier parameter ω ($0 \leq \omega \leq 1$), the parameter β that is used to smooth the Gaussian kernels, and the parameter λ that is used to control the roles of the regularization term, as illustrated as equation (11). For a fair comparison, we adopt same settings of these parameters and remain unchanged in the following experiments, which are $\omega = 0.7$, $\beta = 2$ and $\lambda = 10$. For GLTP, we use the authors' recommended parameter settings, and also keep these settings unchanged in the experiments.

A. Results on wolf dataset

In this experiment, we use the wolf shapes of the TOSCA 3D point data in [40] to compare the performance of CPD, GLTP and the proposed algorithm on accuracy and efficiency. The wolf dataset contains 3 shapes ('wolf0', 'wolf1', and 'wolf2') in different poses, and each shape has 4344 points. The wolf shapes are renormalized into $[-1, 1]$. We employ wolf0 as the model point set, wolf1 and wolf2 as the scene point sets. Wolf0 and wolf1, wolf0 and wolf2 are defined as Group I and Group II, respectively. We introduce four kinds of data degradations, including nonrigid deformation, noise, occlusion and outliers, to evaluate the performance of the registration methods on accuracy and efficiency. All the methods run 100 iterations.

Fig. 1(a) and (b) show the registration results of fast-CPD between wolf0 and wolf1 (Group I), wolf0 and wolf2 (Group II). Notably, the attitude change between wolf0 and wolf1 is large. We can see that fast-CPD can both well align the two groups of point sets. Next, we add Gaussian white noise to wolf1 and wolf2 to make the points randomly deviate their original positions. The mean of the noise is zero and the standard deviation is 0.1. As shown in Fig.1 (c) and (d), fast-CPD still can well recover the spatial transformation between the point sets, although there is noise pollution in the data. As demonstrated in [15], there are two cases in the degradation of occlusion, which are missing points on one side and on both sides. According to equation (5), the corresponding constraint that is introduced for fast-CPD is to force each model point to search its corresponding point in the other point set. When there are missing points in the model point set, or there are few missing points in the scene point set, our method can keep good performance. When there are a number of missing points in the scene point set, we can first recover the transformation from the scene point set to the model point set to get accurate one-to-one correspondences, and pick out the corresponding points. Then we can utilize the obtained one-to-one correspondences and the selected points to calculate the spatial transformation

from the model point set to scene point set. Therefore, our method can well handle the first case. However, our method performs not well when there are many missing points on both sides. In the test of occlusion, we present the experiments with missing points on one side. The number of missing points in wolf0 is 1000. As shown in Fig. (e) and (f), we can see that our method can accurately align the model point sets to the scene point sets. In the test of outliers, we add outliers to wolf1 and wolf2, and the ratio of outlier to data is 0.6. The registration results are shown in Fig. (g) and (h). Our method can perform very well under the interference of outliers. Further, we give the quantitative results of CPD, GLTP and ours in TABLE I. As illustrated in TABLE I, in the test of deformation, our method is slightly better than CPD and GLTP. In the test of noise, the registration results of the three methods are almost the same. In the test of occlusion, we can see that CPD gets the best performance in the experiment of Group II, but fails in Group I. GLTP and ours can keep stable performance in both two experiments, and GLTP is slightly more accurate than ours. In the test of outliers, we can see that the registration results of our method are much better than CPD and GLTP. This shows that the corresponding constraint of equation (5) can help the registration methods to improve their performance in the scenarios of outlier degradation.

In TABLE II and TABLE III, we give the comparisons of runtime on the wolf dataset. As illustrated in the two tables, the time t_c for correspondence determination is relevant to the number of model points and scene points. Compared with CPD and GLTP, fast-CPD consumes a little more time (t_c) on correspondence determination because of the extra operations of normalization as illustrated by equation (5). As illustrated by TABLE II and TABLE III, for fast-CPD, the time t_f for spatial transformation retrieval is composed by the time t_{eig} and the time t_{iter} . Before the iteration begins, fast-CPD has to use time t_{eig} to take the eigen-decomposition of the kernel matrix $\Phi \in \mathbb{R}^{M \times M}$ once. Although CPD and GLTP are not necessary to do this, they have to compute the inversion of a $M \times M$ matrix with time complexity $O(M^3)$ in each iteration. Therefore, fast-CPD spends much less time on computing the spatial transformation than CPD and GLTP. By comparing the total time consumption t_{total} , fast-CPD can run more efficiently than CPD and GLTP in various data degradations.

B. Results on bunny dataset

In this experiment, we concentrate on evaluating the computational efficiency of the point set registration methods, including CPD, CPD(low-rank) that is denoted as CPD-L, fast-CPD and fast-CPD(low-rank) that is denoted as fast-CPD-L. We resample the bunny dataset [41] as six sets with different number of points: 4000×3 , 8000×3 , 12000×3 , 16000×3 , 20000×3 and 24000×3 . The original bunny point set is employed as the scene point set. We adopt the version of bunny point set with random affine transformation as the model point set. Each method runs 50 iterations. CPD-L and fast-CPD-L both preserve $K = 0.1M$ largest eigenvalues of the matrix Φ . For CPD-L, it needs $O(K^3)$ operations to compute the spatial transformation in each iteration. Fig. 2 shows the input point sets and the visualization of the registration results. All the methods are successful to achieve the registration with error less than 5×10^{-3} . TABLE IV gives the runtime of the four point set registration methods. In the following, we detailly discuss the results.

- 1) t_c . t_c represents the time consumption that is used to determine the corresponding relationship between the two point sets. As illustrated by the third row of TABLE IV, CPD and CPD-L consume less time on the correspondence determination than fast-CPD and fast-CPD-L because fast-CPD and fast-CPD-L have to take normalization operations as equation (5) with linear computational complexity.

t_{eig} . t_{eig} denotes the time consumption that is used to take the eigen-decomposition of the kernel matrix $\Phi \in \mathbb{R}^{M \times M}$. This operation only needs to be taken once. Besides, it can be precomputed to significantly increase the processing speed when there are many different scene point sets to be matched with several model point sets. In our experiment, the eigen-decomposition of the kernel matrix $\Phi \in \mathbb{R}^{M \times M}$ is calculated in advance. In the experiment, CPD-L, fast-CPD and fast-CPD-L can directly load the corresponding data file so that the three methods have the same t_{eig} .

- 2) t_{iter} . t_{iter} is the time that is consumed to solve the interpolation functions in the iterations. As illustrated by TABLE IV, although the time t_{eig} of CPD is zero, CPD has to take much more time in the iterations because it needs to perform inversion of a $M \times M$ matrix per iteration with time complexity $O(M^3)$. CPD-L is apparently faster than CPD. Compared with CPD and CPD-

L, fast-CPD spends much less time to compute the spatial transformation. By introducing the low-rank approximation, fast-CPD-L can further reduce the time t_{iter} . Notably, fast-CPD-L only needs about 5.1 seconds to calculate the spatial transformation between the point sets that both contain 24000 points, and each iteration just needs about 0.102 seconds.

- 3) t_f . t_f is the sum of t_{eig} and t_{iter} . Although CPD-L, fast-CPD and fast-CPD-L have to take eigenvalue decomposition of $\Phi \in \mathbb{R}^{M \times M}$ once before the iterations, but they save a lot of time in the iterations. Besides, in many scenarios, the eigenvalue decomposition of $\Phi \in \mathbb{R}^{M \times M}$ can be precomputed so that the time of t_f can be further lowered. Additionally, fast-CPD and fast-CPD-L are much faster than CPD-L.
- 4) t_{total} . t_{total} is the total time consumption of the point set registration methods. Because the significantly advantage in the step of spatial transformation recovery, fast-CPD and fast-CPD-L are apparently faster than CPD and CPD-L.

In summary, the proposed methods can significantly accelerate the nonrigid registration process, especially in large-scale problems.

V. Conclusion

In this paper, we propose a fast implementation of CPD, which is namely fast-CPD. The highlight is that our method can avoid the big matrix-inverse operation in each iteration. This can significantly reduce the computational cost. The computational complexity of fast CPD is approximately $O(M^2)$. We can further reduce the computational cost by low-rank approximation. Besides, the modified methods based on CPD can be easily accelerated by our method. The experimental results on 3D point sets show that our method can achieve comparable performance with CPD on accuracy, while it can significantly save the computing time.

The main limitation of the proposed methods is that when there are many miss points are on both sides, our method cannot keep good performance.

ACKNOWLEDGMENT

The authors thank Andriy Myronenko, Xubo Song, Ge Song and Fan Guoliang for providing their source codes and datasets, which greatly facilitated the comparison experiments.

REFERENCES

- [1] P. J. Besl and H. D. McKay, "A method for registration of 3-D shapes," *IEEE Trans. Pattern Anal. Mach. Intell.*, vol. 14, no. 2, pp. 239-256, 1992.
- [2] Z. Zhang, "Iterative point matching for registration of free-form curves and surfaces," *Int. J. Comput. Vis.*, vol. 13, no. 2, pp. 119-152, 1994.
- [3] H. Chui and A. Rangarajan, "A Feature Registration Framework Using Mixture Models," in *Proc. IEEE Workshop Math. Methods in Biomedical Image Analysis.*, 2000, pp. 190-197.
- [4] H. Chui and A. Rangarajan, "A new point matching algorithm for non-rigid registration," *Comput. Vis. Image Underst.*, vol. 89, no. 2-3, pp. 114-141, 2003.
- [5] A. Myronenko, X. Song, and M. A. Carreira-Perpinán, "Non-rigid point set registration: Coherent point drift," in *Advances in neural information processing systems*, 2007, pp. 1009-1016.
- [6] A. Myronenko and X. Song, "Point set registration: Coherent point drift," *IEEE Trans. Pattern Anal. Mach. Intell.*, vol. 32, no. 12, pp. 2262-2275, 2010.
- [7] B. Jian and B. C. Vemuri, "Robust point set registration using gaussian mixture models," *IEEE Trans. Pattern Anal. Mach. Intell.*, vol. 33, no. 8, pp. 1633-1645, 2010.
- [8] Tao W, Sun K. "Robust point sets matching by fusing feature and spatial information using nonuniform Gaussian mixture models." *IEEE Trans. Image Process.*, vol. 24, no. 11, pp. 3754-3767, 2015.
- [9] Wang G, Wang Z, Chen Y. "A robust non-rigid point set registration method based on asymmetric gaussian representation". *Comput. Vis. Image Underst.*, vol. 141, pp. 67-80, 2015.
- [10] Z Zhou, J Tu, C Geng, J Hu, B Tong, J Ji, and Y Dai. "Accurate and robust non-rigid point set registration using student's mixture model with prior probability modeling," *Scientific reports*, vol. 8, no. 1, pp. 8742, 2018.
- [11] Y. Zheng and D. Doermann, "Robust point matching for nonrigid shapes by preserving local neighborhood structures," *IEEE Trans. Pattern Anal. Mach. Intell.*, vol. 28, no. 4, pp. 643-649, 2006.
- [12] J. Ma, J. Zhao, and A. L. Yuille, "Non-rigid point set registration by preserving global and local structures," *IEEE Trans. Image Process.*, vol. 25, no. 1, pp. 53-64, 2015.
- [13] J. Ma, J. Wu, J. Zhao, J. Jiang, H. Zhou, and Q. Z. Sheng, "Nonrigid point set registration with

- robust transformation learning under manifold regularization," *IEEE Trans. Neural Netw. Learn. Syst.*, pp. 1-14, 2018.
- [14] Wang G , Zhou Q , Chen Y . "Robust Non-Rigid Point Set Registration Using Spatially Constrained Gaussian Fields," *IEEE Trans. Image Process.*, vol. 26, no. 4, pp. 1759-1769, 2017.
- [15] Y. Yang, S. H. Ong, and K. W. C. Foong, "A robust global and local mixture distance based non-rigid point set registration," *Pattern Recognit.*, vol. 48, no. 1, pp. 156-173, 2015.
- [16] S. Zhang, K. Yang, Y. Yang, Y. Luo, and Z. Wei, "Non-rigid point set registration using dual-feature finite mixture model and global-local structural preservation," *Pattern Recognit.*, vol. 80, pp. 183-195, 2018.
- [17] S. J. Belongie, J. Malik, and J. Puzicha, "Shape matching and object recognition using shape contexts," *IEEE Trans. Pattern Anal. Mach. Intell.*, vol. 24, no. 4, pp. 509-522, 2002.
- [18] H. Ling and D. W. Jacobs, "Shape classification using the inner-distance," *IEEE Trans. Pattern Anal. Mach. Intell.*, vol. 29, no. 2, pp. 286–299, Feb. 2007.
- [19] R. B. Rusu, N. Blodow, and M. Beetz, "Fast point feature histograms (FPFH) for 3D registration," in *Proc. IEEE Int. Conf. Robot. Autom.*, May 2009, pp. 3212–3217.
- [20] A. Frome, D. Huber, R. Kolluri, T. Bülow, and J. Malik, "Recognizing objects in range data using regional point descriptors," *Lect. Notes Comput. Sci.*, vol. 3023, pp. 224–237, 2004.
- [21] L. Bai, X. Yang, and H. Gao, "Nonrigid point set registration by preserving local connectivity," *IEEE T. Cybern.*, vol. 48, no. 3, pp. 826-835, 2017.
- [22] S. Ge, G. Fan, and M. Ding, "Non-rigid point set registration with global-local topology preservation," in *Proc. IEEE Conf. Comput. Vis. Pattern Recognit.*, 2014, pp. 245-251.
- [23] S. Ge and G. Fan, "Topology-aware non-rigid point set registration via global-local topology preservation," *Mach. Vis. Appl.*, pp. 1-19, 2019.
- [24] Jiayi Ma, Xingyu Jiang, Junjun Jiang, and Yuan Gao. "Feature-guided Gaussian mixture model for image matching", *Pattern Recognit.*, vol. 92, pp. 231-245, 2019.
- [25] J. Ma, J. Zhao, J. Jiang, H. Zhou, and X. Guo, "Locality preserving matching," *Int. J. Comput. Vis.*, vol. 127, no. 5, pp. 512-531, 2019.
- [26] Y. Tsin and T. Kanade, "A correlation-based approach to robust point set registration," in *Proc. Eur. Conf. Comput. Vis.*, Springer, 2004, pp. 558-569.
- [27] T. M. Nguyen and Q. M. J. Wu, "Multiple kernel point set registration," *IEEE Trans. Med.*

- Imag.*, vol. 35, no. 6, pp. 1381-1394, Jun. 2016.
- [28] J. Ma, W. Qiu, J. Zhao, Y. Ma, A. L. Yuille, and Z. Tu, "Robust L2E estimation of transformation for non-rigid registration," *IEEE Trans. Signal Process.*, vol. 63, no. 5, pp. 1115-1129, 2015.
- [29] E. Hasanbelliu, L. S. Giraldo, and J. C. Principe, "A robust point matching algorithm for non-rigid registration using the cauchy-schwarz divergence," in *Proc. IEEE International Workshop on Machine Learning for Signal Processing*, 2011, pp. 1-6
- [30] B. Maiseli, Y. Gu, and H. Gao, "Recent developments and trends in point set registration methods," *J. Vis. Commun. Image Represent.*, vol. 46, pp. 95-106, 2017.
- [31] H. Zhu, B. Guo, K. Zou, Y. Li, K. Yuen, L. Mihaylova, and H. Leung. "A review of point set registration: From pairwise registration to groupwise registration," *Sensors*, vol. 19, no. 5, p. 1191, 2019.
- [32] J. Canny, "A Computational Approach to Edge Detection," *IEEE Trans. Pattern Anal. Mach. Intell.*, no. 6, pp. 679-698, 1986.
- [33] Rosten E, Porter R, Drummond T. "Faster and better: A machine learning approach to corner detection." *IEEE Trans. Pattern Anal. Mach. Intell.*, vol. 32, no. 1, pp. 105–119, 2008.
- [34] D. G. Lowe, "Distinctive image features from scale-invariant keypoints," *Int. J. Comput. Vis.*, vol. 60, no. 2, pp. 91-110, 2004.
- [35] E. Rublee, V. Rabaud, K. Konolige, and G. R. Bradski, "ORB: An efficient alternative to SIFT or SURF," in *Proc. IEEE Int. Conf. Comput. Vis.*, 2011, vol. 11, no. 1.
- [36] Christopher M Bishop. "Pattern Recognition and Machine Learning". *Springer-Verlag New York, Inc.* 2006.
- [37] A.N. Tikhonov and V.I. Arsenin, "Solutions of Ill-Posed Problems," *Winston and Sons*, 1977.
- [38] A.L. Yuille and N.M. Grzywacz, "The Motion Coherence Theory," in *Proc. IEEE Int'l Conf. Computer Vision*, vol. 3, pp. 344-353, 1988.
- [39] A.L. Yuille and N.M. Grzywacz, "A Mathematical Analysis of the Motion Coherence Theory," *Int. J. Comput. Vis.*, vol. 3, no. 2, pp. 155-175, 1989.
- [40] A. M. Bronstein, M. M. Bronstein, R. Kimmel, "Efficient computation of isometry-invariant distances between surfaces", *SIAM J. Scientific Computing*, vol. 28, no. 5, pp. 1812-1836, 2006.
- [41] "The Stanford 3D Scanning Repository," <http://graphics.stanford.edu/data/3Dscanrep/>, 2010.

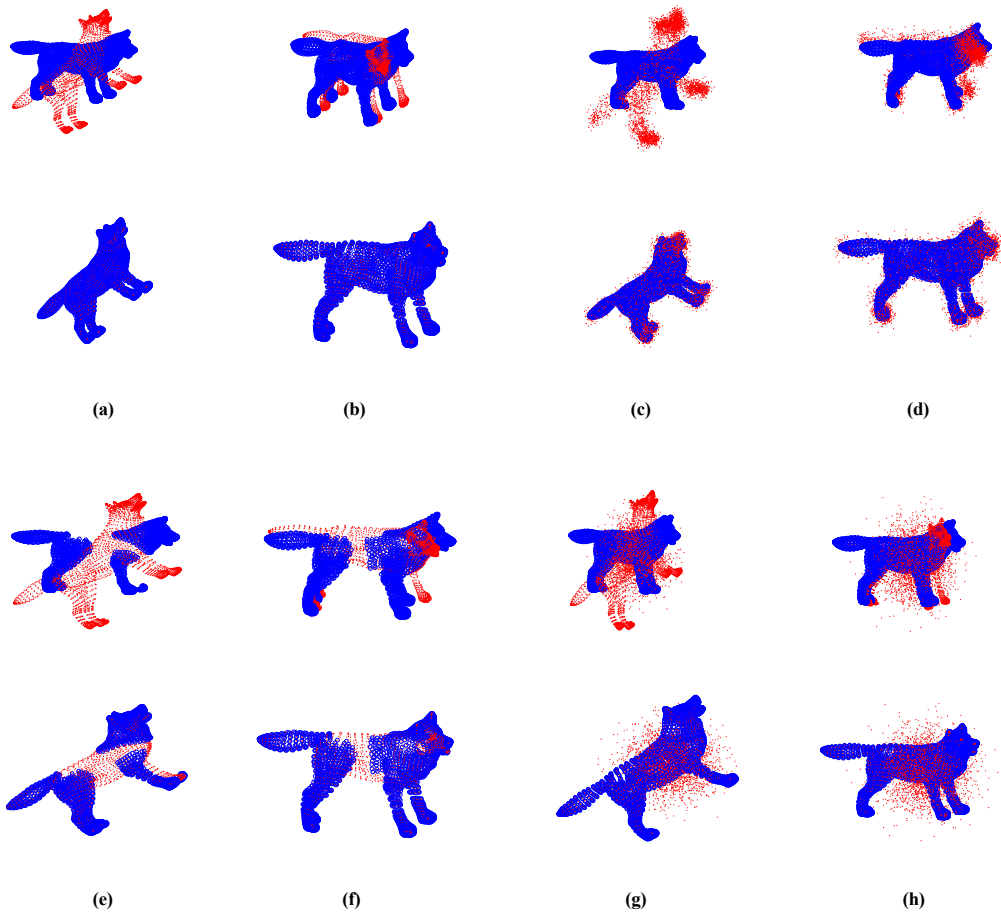


FIGURE 1. Registration results of fast-CPD on wolf dataset. (a)-(b): deformation, (c)-(d): noise, (e)-(f): occlusion, (g)-(h): outliers. (a)(c)(e)(f) belong to Group I, and (b)(d)(f)(h) belong to Group II. The upper row shows the data, and the lower row shows the registration results.

TABLE I RMSE of the point set registration methods on wolf dataset.

		Deformation	Noise	Occlusion	Outliers
Group I	CPD	0.0101	0.0720	0.2239	0.0383
	GLTP	0.0099	0.0715	0.0114	0.0445
	Fast-CPD	0.0087	0.0721	0.0140	0.0090
Group II	CPD	0.0133	0.0715	0.0089	0.0441
	GLTP	0.0113	0.0711	0.0100	0.0496
	Fast-CPD	0.0097	0.0715	0.0102	0.0103

TABLE II Runtime (s) of the point set registration methods on wolf dataset of Group I.

		t_c	t_{eig}	t_{iter}	t_f	t_{total}
Deformation	CPD	35.141	0	64.706	64.706	102.636
	GLTP	35.445	0	86.706	86.706	124.654
	Fast-CPD	37.097	5.808	1.733	7.541	47.037
Noise	CPD	38.305	0	63.725	63.725	63.725
	GLTP	38.205	0	87.395	87.395	127.608
	Fast-CPD	40.103	5.830	1.747	7.577	50.182
Occlusion	CPD	29.143	0	34.880	34.880	65.773
	GLTP	28.103	0	48.316	48.316	78.047
	Fast-CPD	29.207	2.518	1.062	3.58	34.396
Outliers	CPD	59.682	0	63.399	63.399	125.761
	GLTP	59.977	0	86.705	86.705	148.885
	Fast-CPD	61.979	5.828	1.776	7.604	72.120

TABLE III Runtime (s) of the point set registration methods on wolf dataset of Group II.

		t_c	t_{eig}	t_{iter}	t_f	t_{total}
Deformation	CPD	34.895	0	64.417	64.417	101.954
	GLTP	35.850	0	88.942	88.942	127.039
	Fast-CPD	36.819	5.805	1.742	7.547	46.881
Noise	CPD	37.275	0	62.573	62.573	102.418
	GLTP	37.416	0	87.225	87.225	126.510
	Fast-CPD	39.336	5.735	1.755	7.49	49.335
Occlusion	CPD	27.275	0	34.600	34.600	63.636
	GLTP	27.791	0	48.476	48.476	77.911
	Fast-CPD	28.362	2.589	1.042	3.631	33.571
Outliers	CPD	59.842	0	63.927	63.927	127.476
	GLTP	60.117	0	87.591	87.591	149.912
	Fast-CPD	61.788	5.733	1.785	7.518	71.826



FIGURE 2. Registration results of fast-CPD on bunny dataset with 4000 points. Left: the origin data. Right: the registration results.

TABLE IV Runtime (s) of the point set registration methods on bunny dataset.

Number of points		t_c	t_{eig}	t_{iter}	t_f	t_{total}
4000	CPD	15.257	0	27.529	27.529	44.161
	CPD-L	14.754	4.580	6.226	10.806	26.570
	Fast-CPD	16.105	4.580	0.809	5.389	23.157
	Fast-CPD-L	16.057	4.580	0.106	4.686	22.359
8000	CPD	61.283	0	161.938	161.938	228.066
	CPD-L	61.375	34.301	43.395	77.696	141.496
	Fast-CPD	65.920	34.301	3.297	37.598	108.800
	Fast-CPD-L	66.143	34.301	0.374	34.675	105.812
12000	CPD	136.828	0	480.412	480.412	628.192
	CPD-L	137.258	113.351	125.135	238.486	380.742
	Fast-CPD	150.717	113.351	8.734	121.725	284.480
	Fast-CPD-L	148.652	113.351	0.766	114.117	273.534
16000	CPD	240.522	0	1090.468	1090.468	1353.219
	CPD-L	243.605	256.055	279.499	553.554	787.932
	Fast-CPD	262.316	256.055	17.887	273.942	557.880
	Fast-CPD-L	265.928	256.055	1.713	257.768	543.163
20000	CPD	373.064	0	2045.739	2045.739	2457.879
	CPD-L	373.195	502.663	523.244	1025.907	1416.212
	Fast-CPD	418.746	502.663	34.592	537.255	988.430
	Fast-CPD-L	415.051	502.663	3.540	506.203	956.779
24000	CPD	551.761	0	3474.422	3474.422	4119.303
	CPD-L	553.102	852.925	905.934	1758.295	2364.277
	Fast-CPD	630.526	852.925	47.302	900.227	1602.056
	Fast-CPD-L	615.869	852.925	5.131	858.056	1545.760